Materials Science

http://www.aimspress.com/journal/Materials/

AIMS Materials Science, 3(1): 149–159
DOI: 10.3934/matersci.2016.1.149
Received: 20 December 2016
Accepted: 11 January 2016
Published: 18 January 2016

Research article

Modified Becke-Johnson exchange potential: improved modeling of lead halides for solar cell applications

Radi A. Jishi

Department of Physics, California State University, Los Angeles, California, U.S.A; Email: rjishi@calstatela.edu; Tel:323-343-2137.

Abstract: We report first-principles calculations, within density functional theory, on the lead halide compounds $PbCl_2$, $PbBr_2$, and $CH_3NH_3PbBr_{3-x}Cl_x$, taking into account spin-orbit coupling. We show that, when the modified Becke-Johnson exchange potential is used with a suitable choice of defining parameters, excellent agreement between calculations and experiment is obtained. The computational model is then used to study the effect of replacing the methylammonium cation in $CH_3NH_3PbI_3$ and $CH_3NH_3PbBr_3$ with either $N_2H_5^+$ or $N_2H_3^+$, which have slightly smaller ionic radii than methylammonium. We predict that a considerable downshift in the values of the band gaps occurs with this replacement. The resulting compounds would extend optical absorption down to the near-infrared region, creating excellent light harvesters for solar cells.

Keywords: DFT; lead halides; mBJ; perovskites; photovoltaics; solar cells; spin-orbit

1. Introduction

Organolead halide perovskites are attracting great interest, mainly because of their photovoltaic applications. These compounds have the general formula ABX_3, where A is an organic cation, B is lead, and X is a halide ion. An example is methylammonium lead iodide ($CH_3NH_3PbI_3$, abbreviated as $MAPbI_3$), where the MA ion is coordinated to 12 I ions, while Pb is octahedrally coordinated to six I ions, with every two adjacent octahedra sharing a corner.

Following publication of the first report [1] on the use of these compounds as light harvesters in photovoltaic cells, many experimental studies have tried to improve upon material preparation methods and enhance their solar-to-electric power conversion efficiency. [2–14] Theoretical studies have also been undertaken to explore the electronic properties of these compounds and to develop accurate models for computing the energy bands. [15–25]

$MAPbI_3$ has a band gap of 1.5-1.6 eV. [12, 26] The possibility of tuning the band gap by various substitutions has been considered. One approach is to replace I with Br or Cl, yielding $MAPbBr_3$ or

$MAPbCl_3$, with band gaps given by 2.22 eV and 3.17 eV, respectively.[12, 27, 28] Another approach is to replace the methylammonium cation with another cation of a different size. When CH_3NH_3 is replaced with FA = NH_2CHNH_2 (formamidinium), $FAPbI_3$ with a band gap of 1.43-1.48 eV is obtained. [29–33] The lower band gap in $FAPbI_3$, compared to the one in $MAPbI_3$, leads to an increase in the material's optical absorption range. Unfortunately, $FAPbI_3$ is unstable under ambient conditions. However, it has been shown recently that the incorporation of $MAPbBr_3$ into $FAPbI_3$ stabilizes the perovskite phase of $FAPbI_3$ and enhances the power conversion efficiency of the solar cell to 18 percent.[34]

In addition to the extensive work demonstrating the applications of organometallic halides in solar cells, it has been shown that these materials have optoelectronic applications in light-emitting diodes.[35, 36] For such applications, it is desirable to have materials where the optical band gap can be tuned over a wide range of the visible spectrum. Recent studies [27] have shown that, in $MAPbBr_3$, it is easy to substitute Cl for Br, yielding air-stable $MAPbBr_{3-x}Cl_x$ with x=0-3. The simple cubic lattice structure of $MAPbBr_3$ is maintained as x increases, and the lattice constant decreases linearly with increasing x; the reduction is 5% at $x = 3$. On the other hand, the band gap increases with increasing x, leading to a tunable band gap in the 400 to 550 nm wavelength range.

The crystal structure of the organometallic halides depends on the radii of the constituent ions through the Goldschmidt tolerance factor t, which, for the compound ABX_3, is given by

$$t = \frac{r_A + r_X}{\sqrt{2}(r_B + r_X)} \tag{1}$$

where r_A, r_B, and r_X are the ionic radii of the A, B, and X ions, respectively. This factor serves as a guide to predicting the crystal structure of ABX_3; for values of t ranging from 0.9 to 1.0, an ideal cubic perovskite structure is favored.

In calculating t, one is faced with the problem of what value to use for the ionic radius of the organic cation A; different values result from different methods of calculation. Amat et al.[37] obtained an ionic radius of 2.70 Å for $CH_3NH_3^+$ by calculating the volume inside a contour of 0.001 electrons/bohr^3 density. Kieslich et al.[38] considered a hard sphere model in which the cation rotates freely about its center of mass. The ionic radius of $CH_3NH_3^+$ is then taken to be the distance from the cation's center of mass to nitrogen, plus 1.46 Å (the ionic radius of nitrogen). This method yields a value of 2.17 Å for the ionic radius of the methylammonium ion.

We can set some bounds on the value of the ionic radius of $CH_3NH_3^+$ by noting that both $MAPbBr_3$ and $MAPbCl_3$ adopt an ideal cubic perovskite structure. Taking the ionic radii of Pb, Br, and Cl to be 1.19 Å, 1.96 Å, and 1.81 Å, respectively, we find that for the tolerance factor t to lie between 0.9 and 1.0, the ionic radius of $CH_3NH_3^+$ should lie between 2.04 Å and 2.50 Å, These values should not be considered strict limits; they are reasonable estimates. We should note that, in organolead halide compounds, the methylammonium ion does not rotate freely about its center of mass. There is disorder, manifested by the existence of 12 equivalent positions for C and N. In all these positions, the midpoint of the C-N bond is always at, or extremely close to, the center of the cubic unit cell.[39] Thus, we may estimate the ionic radius of $CH_3NH_3^+$ as one half the C-N bond length plus the ionic radius of nitrogen. Optimizing the structure of the methylammonium cation by using the 6-31G** basis set of gaussian orbitals and the B3LYP exchange potential [40] as implemented within Gaussian 09, [41] the ionic radius of the cation is found to be 2.23 Å. The resulting Goldschmidt tolerance factors are 0.952,

0.941, and 0.924 for $MAPbCl_3$, $MAPbBr_3$, and $MAPbI_3$, respectively. These values are consistent with the fact that these compounds adopt a perovskite structure.

The electronic properties of organometallic halides depend on various factors which can be controlled experimentally. These factors include lattice constants, which can be varied by applying external pressure or internal chemical pressure; the type of halide ion, controlled by chemical substitution; and the type of organic ion. To obtain meaningful results, it is important to use a computational model which accurately describes the known electronic properties of these compounds and which can predict the effect of these variables upon them. Density functional theory (DFT) in the Kohn-Sham formulation [42] is the most widely used method. Here, the exchange potential is approximated by a functional of the electronic density, with the most common approximations being the local density approximation (LDA) [42] and the generalized gradient approximation (GGA). [43] Although the ground state is well described by LDA and GGA, these approximations fail to account for excited-state properties. In many semiconductors the values of the band gaps are severely underestimated. Improved values for the band gaps are obtained by using the GW method.[44] The usefulness of this method, however, is hampered by its high computational cost.

A different exchange potential, introduced by Becke and Johnson, [45] was recently modified by Tran and Blaha.[46] The modified Becke-Johnson (mBJ) potential is given by

$$V_{mBJ}(\mathbf{r}) = cV_x^{BR}(\mathbf{r}) + (3c-2)\frac{1}{\pi}\sqrt{\frac{5}{12}}\,[2t(\mathbf{r})/\rho(\mathbf{r})]^{1/2} \tag{2}$$

where $V_x^{BR}(\mathbf{r})$ is the Becke-Roussel exchange potential,[47] $\rho(\mathbf{r})$ is the electron density, and $t(\mathbf{r})$ is the Kohn-Sham kinetic energy density. In the above equation,

$$c = A + B\sqrt{g} \tag{3}$$

where g is the average of $|\nabla\rho/\rho|$ over the volume of the unit cell, and A and B are parameters adjusted to produce the best fit to the experimental values of the semiconductor band gaps.

We have recently shown that, upon using the modified Becke-Johnson exchange potential with $A = 0.4$ and $B = 1.0$ bohr$^{1/2}$, the calculated band gaps of $MAPbI_3$, $MAPbBr_3$, $RbPbI_3$, and $CsPbX_3$ (X = Cl, Br, I) are in excellent agreement with experimental values. [24] In this work, we show that applying this method to the lead halide compounds $PbCl_2$, $PbBr_2$, and $MAPbBr_{3-x}Cl_x$ for $x = 1, 2$, and 3 produces accurate values for the band gaps. We then use this method to demonstrate that a small reduction in the lattice constants of $MAPbBr_3$ and $MAPbI_3$ produces a considerable downshift in the band gaps. Reduction in the lattice constants can be achieved by replacing $CH_3NH_3^+$ with slightly smaller cations, such as $N_2H_5^+$ and $N_2H_3^+$.

2. Methods

Total energy calculations are carried out using the all-electron, full potential, linearized augmented plane wave (FP-LAPW) method as implemented in the WIEN2k code.[48] In this method, space is divided into two regions. One region consists of the interior of non-overlapping muffin-tin spheres centered at the atom sites. The rest of the space (the interstitial) constitutes the other region. In all the calculations reported in this work, the radii of the muffin-tin spheres are $2.1a_0$ for Pb, Cl, Br, and I,

where a_0 is the Bohr radius. On the other hand, the radii for C, N, and H are chosen such that the muffin-tin spheres on adjacent atoms almost touch. The electronic wave function is expanded in terms of a set of basis functions which take different forms in the two regions mentioned above. Inside the muffin-tin spheres, the basis functions are atomic-like functions which are expanded in terms of spherical harmonics up to $l_{max} = 10$. In the interstitial region, they are plane waves with a maximum wave vector K_{max}. Each plane wave is augmented by one atomic-like function in each muffin-tin sphere. Usually, K_{max} is chosen such that $R_{mt}K_{max}$ = 6-9, where R_{mt} is the radius of the smallest muffin-tin sphere in the unit cell. However, due to the very smallness of the muffin-tin radius of hydrogen (R_H = 0.65-0.70 a_0), we set $R_H K_{max} = 3.0$. For orthorhombic and tetragonal systems, a 4x4x4 Monkhorst-Pack grid [49] was used for sampling the Brillouin zone, while an 8x8x8 grid was chosen for cubic systems.

The charge density is Fourier-expanded up to a maximum wave vector $G_{max} = 20a_0^{-1}$. In GGA calculations, PBEsol functional [50] is used for the exchange potential. This method is well-suited for optimizing atomic positions and lattice constants. In the self-consistent calculations, the total energy and charge were converged to within 0.1 mRy and 0.001 e, respectively. In calculations which employ the modified Becke-Johnson exchange potential, we choose $A = 0.4$ and $B = 1.0$ bohr$^{1/2}$, where A and B are the parameters which appear in Eq.(3).

3. Results and Discussion

We begin by carrying out DFT calculations on $PbCl_2$, $PbBr_2$, and $MAPbBr_{3-x}Cl_x$, for $x = 0, 1, 2,$ and 3. At room temperature, $PbCl_2$ and $PbBr_2$ adopt an orthorhombic crystal structure [51] with space group Pbnm, while $MAPbBr_{3-x}Cl_x$ crystals have a cubic unit cell [12, 27]. The experimental values of the lattice constants of these crystals are given in Table 1.

Table 1. Crystal structure and lattice constants for some of the compounds studied in this work.

Compound	Structure	Lattice constants (Å)
$PbCl_2$	Orthorhombic	a=9.03, b=7.608, c=4.525
$PbBr_2$	Orthorhombic	a=9.466, b=8.068, c=4.767
$MAPbBr_3$	Cubic	a=5.933
$MAPbBr_2Cl$	Cubic	a=5.88
$MAPbBrCl_2$	Cubic	a=5.78
$MAPbCl_3$	Cubic	a=5.71

In DFT calculations, it is important to take into account spin-orbit coupling, mainly because of the presence of Pb. Our results are summarized in Table 2. In all the compounds under consideration, we find that GGA+SOC severely underestimates the values of the band gaps. On the other hand, our present method (mBJ+SOC, with $A = 0.4$ and $B = 1.0$ bohr$^{1/2}$ in Eq. (3)) yields values for the band gaps which are in excellent agreement with experiment. These results, along with previous calculations [24] on other lead halide compounds, give us confidence in the ability of DFT combined with the mBJ exchange potential to accurately predict the band gaps in all lead halide compounds.

In Fig.1 we present the calculated density of states in $PbBr_2$. The figure shows that the lower-lying conduction bands are derived from Pb orbitals, while both Pb and Br orbitals contribute to the highest

Table 2. Calculated and experimental band gaps, in eV, for the compounds that are studied in this work.

Compound	GGA+SOC	mBJ+SOC	Experiment
$PbCl_2$	3.18	5.13	5.38, [52] 4.86 [53]
$PbBr_2$	2.46	4.19	4.23, [54] 4.1 [55]
$MAPbBr_3$	0.45	2.23	2.28 [12]
$MAPbBr_2Cl$	0.46	2.42	2.65 [27]
$MAPbBrCl_2$	0.57	2.76	2.90 [27]
$MAPbCl_3$	1.0	3.22	3.17 [27]

valence band. The situation is similar in $PbCl_2$ and $MAPbBr_{3-x}Cl_x$; the low conduction bands are derived mainly from Pb orbitals while the valence band is composed of Pb and halide orbitals.

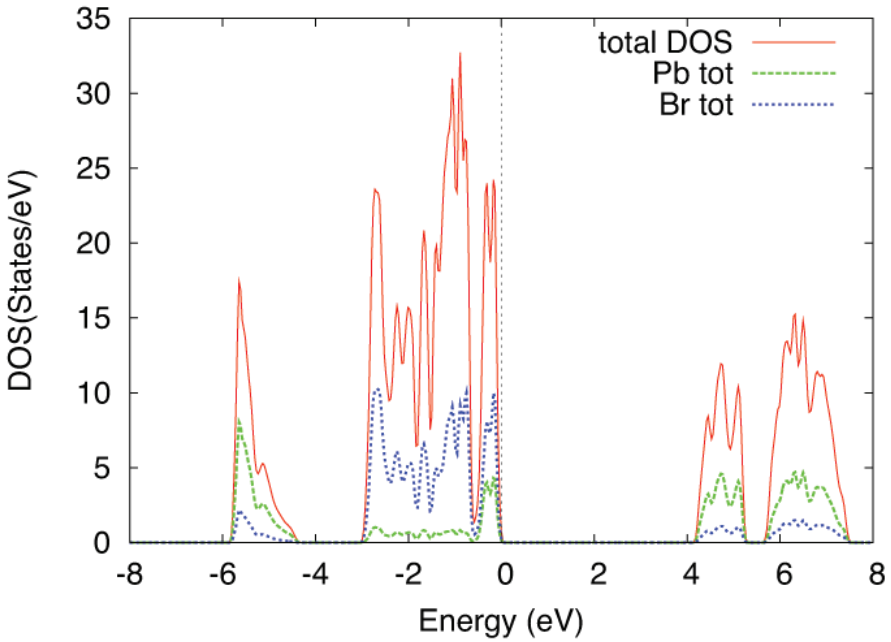

Figure 1. Density of states (DOS) of $PbBr_2$, obtained using the mBJ potential, with A and B in Eq.(3) given by 0.4 and 1.0 $bohr^{1/2}$, respectively, and taking into account the effect of spin-orbit coupling.

We now apply this method to study the variation of the band gap in $MAPbBr_3$ and $MAPbI_3$ with the reduction of the lattice constants. Our results indicate that the band gap in these materials is very sensitive to lattice constant variation. At the experimental values of the lattice constants, our calculations give a band gap of $E_g = 1.54$ eV in $MAPbI_3$ and $E_g = 2.23$ eV in $MAPbBr_3$. For a 1% reduction in the lattice constants, we obtain $E_g = 1.31$ eV in $MAPbI_3$ and $E_g = 1.95$ eV in $MAPbBr_3$, while for a 2% reduction, we obtain $E_g = 1.17$ eV in $MAPbI_3$ and $E_g = 1.75$ eV in $MAPbBr_3$. In arriving at these results, we have assumed that, with reduced lattice constants, $MAPbI_3$ maintains its body-centered tetragonal structure, and $MAPbBr_3$ its simple cubic structure.

A reduction in the lattice constants of organometallic halides can be achieved by applying an exter-

Table 3. Band gaps for different lead halide compounds, calculated using the modified Becke-Johnson exchange potential and taking into account the effect of spin-orbit coupling.

Compound	Band gap (eV)
$N_2H_5PbBr_3$	1.94
$N_2H_3PbBr_3$	1.77
$N_2H_5PbI_3$	1.41
$N_2H_3PbI_3$	1.13

nal pressure or by replacing $CH_3NH_3^+$ with a cation of a slightly smaller ionic radius. We consider two cations: $N_2H_5^+$ (diazanium) and $N_2H_3^+$ (diazenium). In each case, the ionic radius is taken to be equal to one-half the N-N bond length plus the ionic radius of nitrogen, as discussed in the introduction. Using coupled cluster theory with a perturbative treatment of the triple excitations, Matus et al.[56] calculated the N-N bond lengths in $N_2H_5^+$ and $N_2H_3^+$ to be 1.46 Å and 1.24 Å, respectively. Using these values, we obtain 2.19 Å and 2.08 Å for the ionic radii of $N_2H_5^+$ and $N_2H_3^+$, respectively. These values are only slightly smaller than the corresponding value for $CH_3NH_3^+$, estimated by the same method to be 2.23 Å. The Goldschmidt tolerance factors for $N_2H_5PbBr_3$ and $N_2H_5PbI_3$ are 0.932 and 0.916, respectively, while for $N_2H_3PbBr_3$ and $N_2H_3PbI_3$ they are 0.907 and 0.893, respectively. Thus, the replacement of CH_3NH_3 with N_2H_5 or N_2H_3 leads to only a small change in the tolerance factor. Hence, we assume that $N_2H_5PbBr_3$ and $N_2H_3PbBr_3$ will have a cubic unit cell, similar to $MAPbBr_3$, and that $N_2H_5PbI_3$ and $N_2H_3PbI_3$ will maintain a body-centered tetragonal structure, as seen in $MAPbI_3$.

Upon carrying out structure optimization, we find that the lattice constants for $N_2H_5PbBr_3$ and $N_2H_3PbBr_3$ are $a = 5.86$ Å and 5.806 Å, respectively. On the other hand, we find $a = 8.81$ Å and $c = 12.59$ Å for $N_2H_5PbI_3$, while $a = 8.76$ Å and $c = 12.52$ Å for $N_2H_3PbI_3$. The calculated band gaps of these compounds, using the modified Becke-Johnson exchange potential with $A = 0.4$ and $B = 1.0$ bohr$^{1/2}$ in Eq.(3) and taking into account spin-orbit coupling, are presented in Table 3. These results show that the replacement of CH_3NH_3 with N_2H_5 or N_2H_3 causes a considerable redshift in the band gap values.

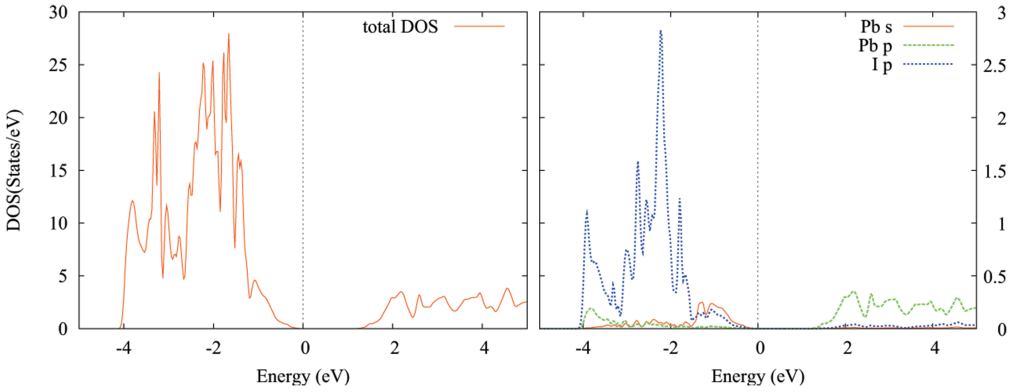

Figure 2. Density of states (DOS) of $N_2H_5PbI_3$, obtained using the mBJ exchange potential and taking into account the effect of spin-orbit coupling.

The calculated density of states in $N_2H_5PbI_3$ is presented in Fig. 2. It is noted that, similar to

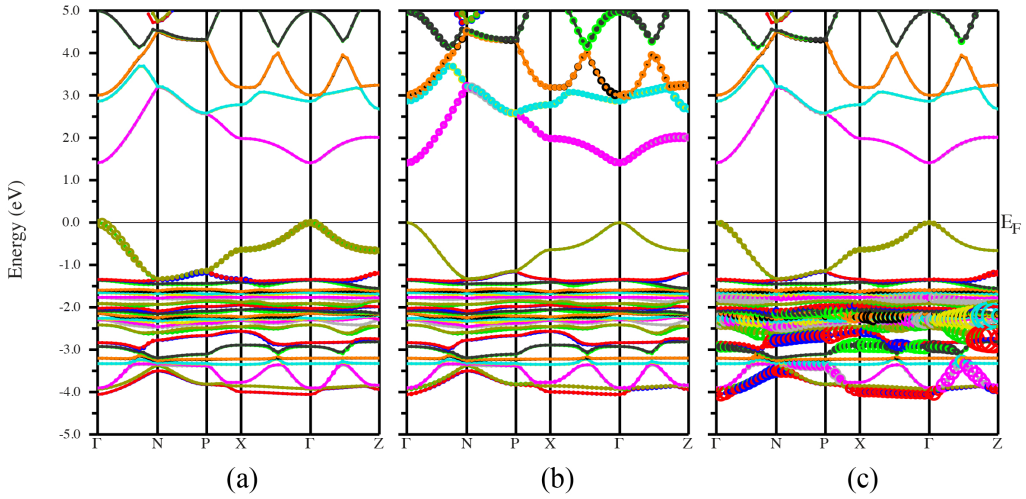

Figure 3. Orbital character of the valence and conduction bands of $N_2H_5PbI_3$. The contribution of the selected orbital to the wave function (in a given band and at a given **k**-point) is proportional to circle size, with a single point denoting zero contribution. (a) Pb 6s orbital, (b) Pb 6p orbital, and (c) I 5p orbital.

$CH_3NH_3PbI_3$, the low-lying conduction bands are derived mainly from Pb p orbitals, whereas the highest valence band is composed of both Pb s and I p states. Bands in the energy range -4 eV to -2 eV are derived mostly from iodine p orbitals. The character of the valence and conduction bands is also made clear in Fig. 3, where the energy bands along some high-symmetry directions in the first Brillouin zone are plotted. The size of the circles is proportional to the contribution of the chosen atomic orbital to the eigenstates at each **k**-point. The fact that s ($l = 0$) and p ($l = 1$) orbitals on the same atom (Pb) make large contributions to the wave functions at the valence band maximum and conduction band minimum is responsible for the large optical absorption coefficients that occur in these compounds, and hence their usefulness in solar cell applications.

In $N_2H_5PbI_3$, the valence band maximum (VBM) and conduction band minimum (CBM) occur at the Γ-point, the Brillouin zone center. In ideal cubic perovskites, VBM and CBM occur at the zone's corner point R(1/2, 1/2, 1/2). Here, $N_2H_5PbI_3$ is assumed to have a body-centered tetragonal structure with two formula units per primitive cell. The conventional tetragonal unit cell, with four formula units, is a slight distortion of the $\sqrt{2} \times \sqrt{2} \times 2$ supercell of the ideal cubic unit cell, and point R is zone-folded into point Γ.

Spin-orbit coupling (SOC) has a profound effect on the band structure in organolead halide compounds. In Fig. 3, we see that at the Γ point, the lowest conduction band has energy 1.41 eV, while the next two higher bands have energy close to 3 eV.. In the absence of SOC, those three bands would be almost degenerate at the Γ point, and all of them would occur at about 2.5 eV. In a cubic perovskite structure, such as the one found in $MAPbBr_3$, the conduction band minimum at point R is six-fold degenerate (including spin degeneracy); SOC partially lifts the degeneracy, giving rise to a doublet ($j = 1/2$) with a lower energy and a quartet ($j = 3/2$) with a higher energy. In a body-centered tetragonal structure, CBM occurs at point Γ, degeneracy is now only approximate (it was exact in the cubic structure), and SOC again splits the almost six-fold degenerate level into one lower doublet and two higher doublets.

4. Conclusions

We have presented calculations on various lead halide compounds using density functional theory with modified Becke-Johnson exchange potential. For the compounds $PbCl_2$, $PbBr_2$, and $CH_3NH_3PbBr_{3-x}Cl_x$, for $x = 0, 1, 2$, and 3, we showed that the calculated band gaps are in excellent agreement with experimental values. We then used this computational method to predict the electronic structure of similar compounds, namely, those that result from the replacement of the methylammonium cation in $MAPbBr_3$ and $MAPbI_3$ with the slightly smaller cations $N_2H_5^+$ and $N_2H_3^+$. A significant downshift in the band gap values is predicted to occur as a result of these replacements. In particular, we predict that $N_2H_5PbI_3$ and $N_2H_3PbI_3$ have band gaps given by 1.41 eV and 1.13 eV, respectively. Therefore. these compounds, if synthesized, would be excellent light harvesters in solar cells. It should be noted, however, that the instability of the diazenium cation ($N_2H_3^+$) may make it difficult to use it as a replacement for the methyl ammonium cation.

Acknowledgments

The author gratefully acknowledges support by National Science Foundation under grant No. HRD-0932421 and NSF PREM Program: Cal State L.A. & Penn State Partnership for Materials Research and Education, award DMR-1523588.

Conflict of Interest

The author reports no conflict of interest in this research.

References

1 Kojima A, Teshima K, Shirai Y, et al. (2009) Organometal halide perovskites as visible-light sensitizers for photovoltaic cells. *J Am Chem Soc* 131: 6050–6051.

2 Etgar L, Gau P, Xue Z, et al. (2012) Mesoscopic $CH_3NH_3PbI_3/TiO_2$ heterojunction solar cells. *J Am Chem Soc* 134: 17396–17399.

3 Ball J, Lee M, Hey A, et al. (2013) Low-temperature processed meso-superstructured to thin-film perovskite solar cells. *Energy Env Sci* 6: 1739–1743.

4 Heo H, Im S, Noh J, et al. (2013) Efficient inorganic-organic hybrid heterojunction solar cells containing perovskite compound and polymeric hole conductors. *Nat Photonics* 7: 486–491.

5 Kim H-S, Lee J-W, Yantara N, et al. (2013) High efficiency solid-state sensitized solar cell based on submicrometer rutile TiO_2 nanorod and $CH_3NH_3PbI_3$ perovskite sensitizer. *Nano Lett* 13: 2412–2417.

6 Bi D, Yang L, Boschloo G, et al. (2013) Effect of different hole transport materials on recombination in $CH_3NH_3PbI_3$ perovskite-sensitized mesoscopic solar cells. *J Phys Chem Lett* 4: 1532–1536.

7 Cai B, Xing Y, Yang Z, et al. (2013) High performance hybrid solar cells sensitized by organolead halide perovskites. *Energy Env Sci* 6: 1480–1485.

8 Eperon G, Burlakov V, Docampo P, et al. (2014) Morphological control for high performance, solution-processed planar heterojunction perovskite solar cells. *Adv Funct Mater* 24: 151–157.

9 Laban W, Etgar L. (2014) Depleted hole conductor-free lead halide iodide heterojunction solar cells. *Energy Env Sci* 6: 3249–3253.

10 Stranks S, Eperon G, Grancini G, et al. (2013) Electron-hole diffusion lengths exceeding 1 micrometer in an organometal trihalide perovskite absorber. *Science* 342: 341–344.

11 Lee M, Teuscher J, Miyasaka T, et al. (2012) Efficient hybrid solar cells based on meso-superstructured organometal halide perovskites. *Science* 338: 643–647.

12 Noh J, Im S, Heo J, et al. (2013) Chemical management for colorful, efficient, and stable inorganic-organic hybrid nanostructured solar cells. *Nano Lett* 13: 1764–1769.

13 Burschka J, Pellet N, Moon S, et al. (2013) Sequential deposition as a route to high-performance perovskite-sensitized solar cells. *Nature* 499: 316–319.

14 Liu M, Johnston M, Snaith H (2013) Efficient planar heterojunction perovskite solar cells by vapour deposition. *Nature* 501: 395–398.

15 Mosconi E, Amat A, Nazeeruddin M, et al. (2013) First-principles modeling of mixed halide organometal perovskites for photovoltaic applications. *J Phys Chem C* 117: 13902–13913.

16 Wang Y, Gould T, Dobson J, et al. (2014) Density functional theory analysis of structural and electronic properties of orthorhombic perovskite $CH_3NH_3PbI_3$. *Phys Chem Chem Phys* 16: 1424–1429.

17 Umari P, Mosconi E, De Angelis, F (2014) Relativistic GW calculations on $CH_3NH_3PbI_3$ and $CH_3NH_3SnI_3$ perovskites for solar cell applications. *Sci Rep* 4: Article number: 4467.

18 Even J, Pedesseau L, Jancu J, et al. (2013) Importance of spin–orbit coupling in hybrid organic/inorganic perovskites for photovoltaic applications. *J Phys Chem Lett* 4: 2999–3005.

19 Even J, Pedesseau L, Dupertuis M, et al. (2012) Electronic model for self-assembled hybrid organic/perovskite semiconductors: reverse band edge electronic states ordering and spin-orbit coupling. *Phys Rev B* 86: 205301.

20 Even J, Pedesseau L, Katan C (2014) Comments on "density functional theory analysis of structural and electronic properties of orthorhombic perovskite $CH_3NH_3PbI_3$." *Phys Chem Chem Phys* 16: 8697-8698

21 Feng J, Xiao B (2014) Correction to "crystal structures, optical properties, and effective mass tensors of $CH_3NH_3PbI_3$ (X=I and Br) phases predicted from HSE06." *J Phys Chem Lett* 5: 1719-1720.

22 Brivio F, Butler K, Walsh A (2014) Relativistic quasiparticle self-consistent electronic structure of hybrid halide perovskite photovoltaic absorbers. *Phys Rev B* 89: 155024

23 Filippetti A, Mattoni A (2014) Hybrid perovskites for photovoltaics: insights from first principles. *Phys Rev B* 89: 125203

24 Jishi R, Ta O, Sharif A (2014) Modeling of lead halide compounds for photovoltaic applications. *J Phys Chem C* 118: 28344–28349.

25 Motta C, El-Mellouhi F, Kais S, et al. (2015) Revealing the role of organic cations in hybrid halide perovskite $CH_3NH_3PbI_3$. *Nat Commun* 6: 7026.

26 Baikie T, Fang Y, Kadro J, et al. (2013) Synthesis and crystal chemistry of the hybrid perovskite $(CH_3NH_3)PbI_3$ for solid-state sensitised solar cell applications. *J Mater Chem A* 1: 5628–5641.

27 Comin R, Walters G, Thibau E, et al. (2015) Structural, optical, and electronic studies of wide-bandgap lead halide perovskites. *J Mater Chem C* 3: 8839–8843.

28 Buin A, Comin R, Xu J, et al. (2015) Halide-dependent electronic structure of organolead perovskite materials. *Chem Mater* 27: 4405–4412.

29 Pang S, Hu H, Zhang J, et al. (2014) $NH_2CH{=}NH_2PbI3$: An alternative organolead iodide perovskite sensitizer for mesoscopic solar cells. *Chem Mater* 26: 1485–1491.

30 Stoumpos C, Malliakas C, Kanatzidis M (2013) Semiconducting tin and lead iodide perovskites with organic cations: phase transitions, high mobilities, and near-infrared photoluminescent properties. *Inorg Chem* 52: 9019–9038.

31 Stoumpos C, Kanatzidis G (2015) The renaissance of halide perovskites and their evolution as emerging semiconductors. *Acc Chem Res* 48: 2791–2802.

32 Eperon G, Stranks S, Menelaou C, et al. (2014) Formamidinium lead trihalide: a broadly tunable perovskite for efficient planar heterojunction solar cells. *Energy Environ Sci* 7: 982–988.

33 Koh T, Fu K, Fang Y, et al. (2014) Formamidinium-containing metal halide: an alternative material for near-IR absorption perovskite solar cells. *J Phys Chem C* 118: 16458–16462.

34 Jeon N, Noh J, Yang W, et al. (2015) Compositional engineering of perovskite materials for high-performance solar cells. *Nature* 517: 476–480.

35 Tan Z, Moghaddam R, Lai M, et al. (2014) Bright light-emitting diodes based on organometal halide perovskite. *Nature Nanotech* 9: 687–692.

36 Kim Y.-H, Cho H, Heo J, et al. (2015) Multicolored organic/inorganic hybrid perovskite light-emitting diodes. *Adv Mater* 27: 1248–1254.

37 Amat A, Mosconi E, Ronca E, et al. (2014) Cation-induced band-gap tuning in organohalide perovskites: interplay of spin-orbit coupling and octahedra tilting. *Nano Lett* 14: 3608–3616.

38 Kieslich G, Sun S, Cheetham A (2015) An extended tolerance factor approach for organic-inorganic perovskites. *Chem Sci* 6: 3430–3433.

39 Mashiyama H, Kurihara Y, Azetsu T (1998) Disordered cubic perovskite structure of $CH_3NH_3PbX_3$ (X = Cl, Br, I). *J Korean Phys Soc* 32: S156-S158.

40 Becke A (1993) Density-functional thermochemistry. III. The role of exact exchange. *J Chem Phys* 98: 5648–5652.

41 Frisch M, Trucks G, Schlegel H, et al. (2009) Gaussian 09, Gaussian, Inc: Willingford, CT.

42 Kohn W, Sham L (1965) Self-consistent equations including exchange and correlation effects. *Phys Rev* 140: A1133–A1138.

43 Perdew J, Burke K, Ernzerhof M (1996) Generalized gradient approximation made simple. *Phys Rev Lett* 77: 3865–3868.

44 Bechstedt F, Fuchs F, Kresse G (2009) Ab-initio theory of semiconductor band structures: new developments and progress. *Phys Status Solidi B* 246: 1877–1892.

45 Becke A, Johnson E (2006) A simple effective potential for exchange. *J Chem Phys* 124: 221101.

46 Tran F, Blaha P (2009) Accurate band gaps of semiconductors and insulators with a semilocal exchange-correlation potential. *Phys Rev Lett* 102: 226401.

47 Becke A, Roussel M (1989) Exchange holes in inhomogeneous systems: a coordinate-space model. *Phys Rev A* 39: 3761–3767.

48 Blaha P, Schwarz K, Madsen G, et al. (2001) WIEN2K: an augmented plane wave + local orbitals program for calculating crystal properties.

49 Monkhorst H, Pack J (1976) Special points for Brillouin-zone integrations. *Phys Rev B* 13: 5188–5192.

50 Perdew J, Ruzsinzky A, Csonka G, et al. (2008) Restoring the density-gradient expansion for exchange in solids. *Phys Rev Lett* 100: 136406.

51 Wyckoff R (1963) Crystal structures, 2nd ed. (Wiley, New York) Vol. 1.

52 Plekhanov V (2004) Lead halides: electronic properties and applications. *Prog Mater Sci* 49: 787–886.

53 Zaldo C, Solé J, Diéguez E, et al. (1985) Optical spectroscopy of $PbCl_2$ particles embedded in NaCl host matrix. *J Chem Phys* 83: 6197–6200.

54 Plekhanov V (1973) Optical constants of lead halides. *Phys Stat Sol B* 57: K55–K59.

55 Iwanaga M, Watanabe M, Hayashi T (2000) Charge separation of excitons and the radiative recombination process in $PbBr_2$ crystals. *Phys Rev B* 62: 10766–10773.

56 Matus M, Arduengo A, Dixon D (2006) The heats of formation of diazene, hydrazine, $N_2H_3^+$, $N_2H_5^+$, N_2H, and N_2H_3 and the methyl derivatives CH_3NNH, CH_3NNCH_3, and $CH_3HNNHCH_3$. *J Phys Chem A* 110: 10116–10121.

AIMS Press